

Numerical study on Coupled Heat and Mass Transfer in Masonry Wall

Fezzioui Naima¹, Mourad Bendekhis², Mébirika Benyamine³

¹Laboratory Mechanics of Structures, Faculty of Technology, Tahri Mohamed University
BP 417, Bechar, Algeria
fezzioui.naima@univ-bechar.dz

²Laboratory of Energetic in Arid Zones (ENERGARID), Faculty of Technology, Tahri Mohamed University
BP 417, Bechar, Algeria
bendekhis.mourad@univ-bechar.dz

³Laboratory of Reliability of Materials and Structures in the South-FIMAS, Faculty of Technology, Tahri Mohamed University
BP 417, Bechar, Algeria
benyamine.mebirika@univ-bechar.dz

Abstract - This numerical study investigates heat and mass transfer in a date palm concrete masonry wall with cement mortar using the Künzle model, examining steady-state (Dirichlet and Neumann conditions) and transient regimes. Results show boundary conditions significantly influence hygrothermal behavior, with temperature and humidity following linear gradients under Neumann conditions without reaching imposed surface values. Material interfaces exhibit pronounced capillary discontinuities, with date palm concrete showing higher water content (up to 55 kg/m³) than mortar joints (<3 kg/m³). In transient analysis, temperatures stabilize quickly (concrete ~15.5°C, mortar ~17°C) while water content increases progressively. Date palm concrete demonstrates dual functionality as a moisture absorber and thermal insulator, highlighting the importance of understanding material-specific hygrothermal properties for sustainable building design.

Keywords: Heat and mass transfer, masonry, hygro-thermal behaviour, mortar, Date palm concrete

1. Introduction

Buildings are the globe's largest energy consumer and greenhouse gas emitter, according to recent statistics from the International Energy Agency (IEA). The industry accounts for approximately 36% of global energy consumption and 37% of global CO₂ emissions, and it is responsible for becoming the prime driver of energy consumption and climate change [1]. Using sustainable construction materials through focusing on minimizing raw material usage and maximizing energy efficiency is a significant means of reducing greenhouse gas emissions [2]. Date palm concrete, in particular, has significant potential since it has an embodied energy much lower than the conventional materials [3-8].

Masonry, a time-tested and widely employed construction material, continues to be a significant contributor to a wide variety of building uses even in the past few decades [9]. Its economical nature and flexibility render it a sought-after material with bricks and mortars as the components, which possess certain mechanical characteristics and shapes [10, 11]. These can be altered and combined in a multitude of means to yield an array of masonry assemblies, thus making it a strong and flexible choice for modern construction needs [12].

Masonries' moisture content in the walls significantly affects overall building performance, such as energy consumption, structural behavior, durability, and service life [13, 14]. Due to these issues, a number of numerical models have been developed, which are defined by dimensionality, flow regime, chosen moisture potential parameter, and input data requirement. While most studies deal with homogeneous porous media, research on multilayered systems, which prevail in building practice, remains limited and encounters some challenges, in particular the continuity of the driving potential at interfaces [13]. Several theoretical models have been established to describe these transport processes, such as thermal conduction, convective transport, capillary flow, and vapor diffusion. These approaches are fundamentally characterized by their driving potential: moisture content [15-18], relative humidity [19-24], capillary pressure [25-27], or vapor pressure [28-30], respectively, as the primary mechanism for heat and moisture transport in porous materials.

The aim of this study was to examine the effect of different types of binders on the thermohydric behavior of date palm concrete masonry wall using cement mortar. The wall was exposed to typical Mediterranean climate conditions, and its performance was analyzed under steady state and transient regimes.

2. Hygrothermal coupled model

Heat and moisture transfer in porous media is a multifaceted problem in structural engineering with numerous concurrent physical mechanisms. It has been a subject of considerable research interest due to its central importance in building performance.

The Künzel model, which has been widely applied to the simulation of coupled heat and moisture transfer in building materials, employs relative humidity as its driving potential rather than moisture content. Proven by Künzel [19] using laboratory tests under real weather conditions, this reduced method based on the Clausius-Clapeyron equation [31] has worked well in simulating permeable materials. While accurate in the hygroscopic range, the model shows limitations in over-hygroscopic cases [32]. Studies indicate that convective coefficients and adsorption isotherms play significant roles in model accuracy [33], with updated versions being more accurate for building envelopes than other models [34].

Based on assumptions in Künzel's model [35], heat and mass transfer governing equations are derived based on principles of energy and mass balance. The equations are meant to treat the transfer of heat and moisture by more than one process, such as conduction, convection, and vapor diffusion, and are expressed in 2D as:

Mass conservation equation

$$d_z \cdot \xi \cdot \frac{\partial \varphi}{\partial t} + \nabla \cdot g = G \quad (1)$$

$$g = -(\xi D_w \nabla \varphi + \delta_p \nabla(\varphi p_{sat})) \text{ and } \xi = \frac{\partial w}{\partial \varphi} \quad (2)$$

Heat conservation equation

$$d_z \cdot (\rho C_p)_{eff} \cdot \frac{\partial T}{\partial t} + \nabla \cdot g = d_z Q + q_0 \quad (3)$$

$$q = -d_z (k_{eff} \nabla T + L_v \delta_p \nabla(\varphi p_{sat})) \quad (4)$$

Where: $\xi = \partial w / \partial \varphi$: specific hygric capacity, D_w : ($m^2 \cdot s^{-1}$) Moisture diffusivity, $\xi D_w = D_l$ ($kg \cdot m^{-2} \cdot s^{-1}$)
 D_l : liquid transfer coefficient under a relative humidity gradient; In hygroscopic region $0 \leq \varphi \leq 95$: $D_l = \left(\frac{1}{\mu(\varphi)^*} - \frac{1}{\mu} \right) (\delta_{p,a} \cdot P_{sat})$; μ and μ^* s the water vapor diffusion resistance fact for wet and dry cup test method described in EN ISO 12572. $\mu = \frac{\delta_{p,a}}{\delta_p}$; $\delta_{p,a}$: Water vapour permeability of air, given by: $\delta_{p,a} = \left(2.306 \cdot 10^{-5} \cdot \frac{P_0}{R_p} \cdot T \cdot P_a \right) (T/273.13)^{1.81}$;
 δ_p : Water vapour permeability

- In the capillary water region, the liquid transfer coefficient, $D_{l,ws}$, is defined as follows:

$$D_{l,ws} = D_{ws} \cdot \xi, \text{ Where : } D_{ws} = 3.8 \left(\frac{A}{W_f} \right)^2 1000^{w/w_f - 1}$$

Interface modeling is very important for the simulation of moisture transport in multi-layered materials like masonry. The interface between different materials is assumed to be a zero-thickness phenomenological zone having either perfect hydraulic contact (having no influence on moisture transport) or imperfect hydraulic contact (causing moisture flux retardation due to pore structure discontinuities or air gaps). Interface permeability is defined in terms of parameters KIF [s/m] or resistance RIF [m/s], and water transport through the interface (gIF) is provided by equations in terms of capillary pressure or relative humidity. These interfaces have zero thickness and no hygroscopic capacity [36-38].

By applying Kelvin's equation, the moisture flow through the interface is given as follows [38]:

$$g_{IF} = \frac{\rho_w R_v T}{\varphi} \frac{\Delta \varphi}{R_{IF}}$$

ρ_w : water density [kg/m³], R_V [J/(kg·K)]: universal gas constant for water vapour.

3. Case study description

The masonry wall chosen for the study is presented in the figure. It consists of bricks with dimensions of 290 mm × 140 mm × 90 mm, with mortar joints of 15 mm thickness. The resulting structure is a masonry wall with a thickness of 395mm and a total height of 2790 mm.

The properties of the materials used for the hygrothermal simulations are presented in Table 1. Two types of mortars were selected to analyze the impact of mortar type on the thermohydric behavior of the wall: cement mortar (CM) and natural hydraulic lime mortar (LM).

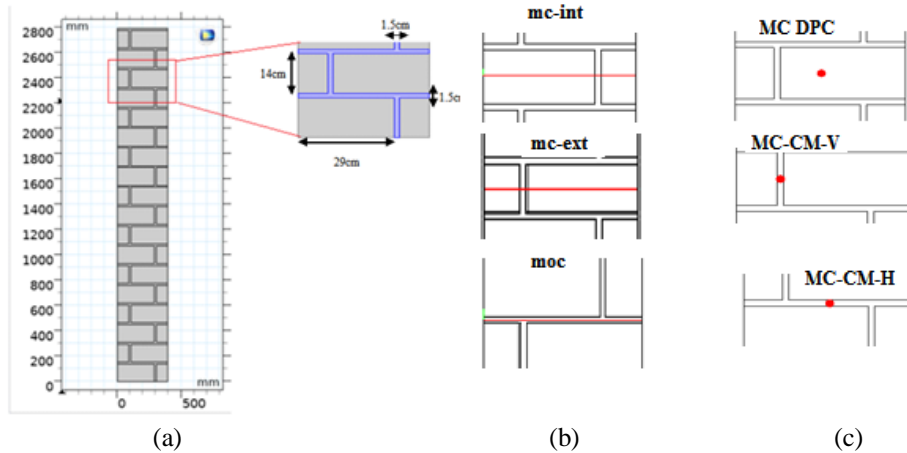


Fig.1: (a) configuration of the studied masonry wall, (b) lines taken for the results of the distribution of T, RH and wc, (c) points taken for the results of the evolution of T, RH and wc.

The material properties used for the hydro-thermal simulations are presented in Table 1.

Table 1: Thermohydric Properties of Bricks and Mortars Used in the Simulation

Property	Specific heat [J kg ⁻¹ K ⁻¹]	Dry thermal conductivity [w m ⁻¹ K ⁻¹]	Vapor resistance factor (wet cap) [-]	Vapor resistance factor (dry cap) [-]	Water adsorption coefficient [kg m ⁻² s ^{-0.5}]	Water content at free saturation [kg m ⁻³]	Dry Density [kg m ⁻³]	Moisture supplement of thermal conductivity [-]
DPC [35]	1500	0.185	5.57	6.310	0.165	429	954	10.19
Cement mortar [28]	932	1.72	25.00		0.060	180	2000	9.29

4. Initial and Boundary conditions

The study is carried out for two regimes: permanent and transient. For the permanent regime, the following initial conditions have been assumed: $T_i = 20^\circ\text{C}$ and $\varphi_i = 50\%$ [19]

For the transient regime, the initial conditions are taken from the permanent state ‘Neumann conditions’.

Two distinct boundary conditions were implemented in this study: Dirichlet conditions for the steady-state analysis (D-SS), and Neumann conditions (N-SS) for the steady-state and transient-state simulations.

Dirichlet conditions : $T_{\text{ext}} = 14^\circ\text{C}$ and $\varphi_{\text{ext}} = 75\%$

Neumann conditions: $Q = h_t(T_{\text{ext}} - T)$, where Q :heat flow density (W/m²), h_t : heat transfer coefficient (W/m².K) takes into account both convection and radiation through the following relation: $h_t = h_r + h_c$; T_{ext} : External temperature

surface (K) and T : wall temperature (K). $h_{t=11.57} \text{ W m}^{-2} \text{ K}^{-1}$ for the interior surface and $h_{t=27} \text{ W m}^{-2} \text{ K}^{-1}$ for the exterior surface [19].

$G_0 = \beta(\varphi_{ext}P_{sat}(T) - \varphi P_{sat}(T))$, with G_0 : convective moisture flow at boundary surface, used for the computation of the vapor saturation pressure. β : moisture transfer coefficient at boundaries. $\beta = 7e - 9 . h_c$. [39]

5. Result and discussion

The numerical simulations were performed by COMSOL Multiphysics software. The influence of mesh refinement on the accuracy of the numerically solved thermal and hydric field is shown through a series of computations with successively finer domain meshes. We compared our numerical model to the experimental work of [38], in which temperature and humidity fields were compared. Figure 3 shows the comparison result with satisfactory agreement.

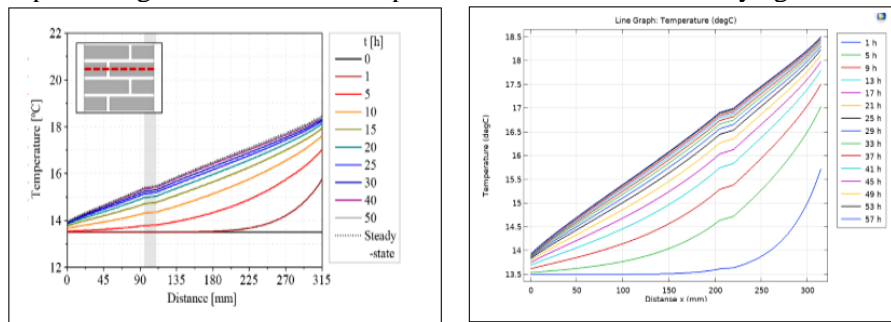
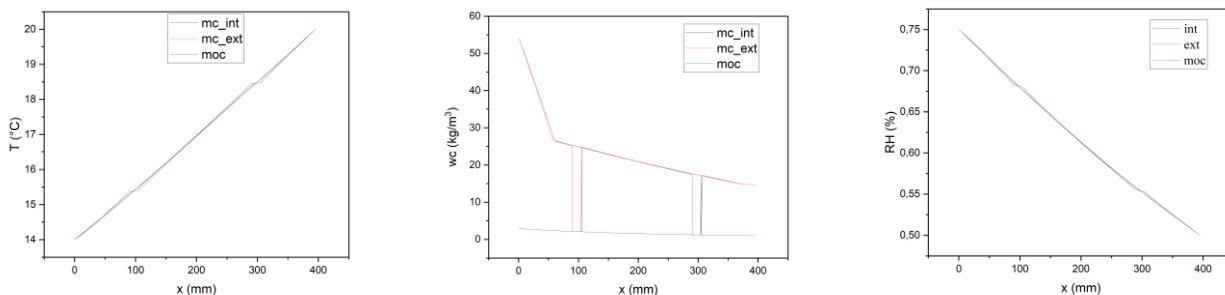
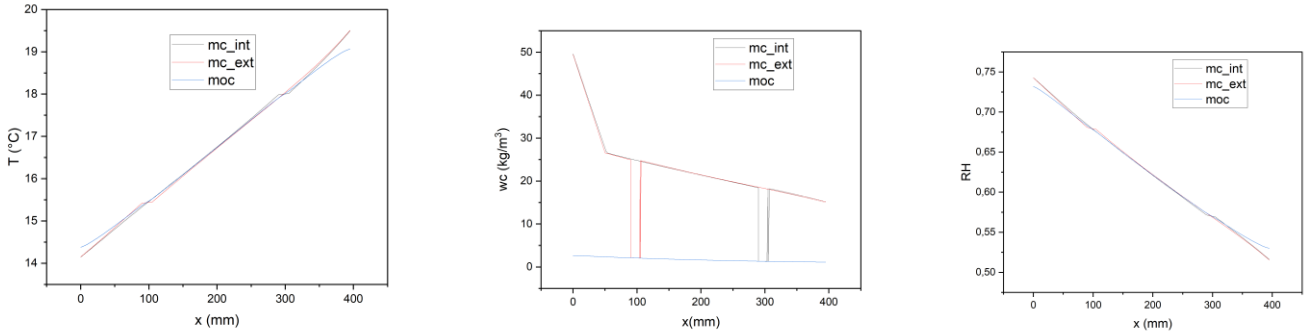


Fig.3 Model Verification Against [38]

The figure 5 shows the temperature, water content and humidity distribution across a masonry wall made of date palm concrete with cement mortar binding for three different lines (mc-int, mc-ext, and moc) as indicated in Fig1. The temperature and humidity distribution strongly depends on the imposed boundary conditions. For the Neumann steady-state conditions (N-SS), the temperature and humidity inside the wall follow a nearly linear gradient. The temperature and relative humidity values in the N-SS case do not attain the values imposed on the wall surfaces, which is evident since the convective heat transfer and convective mass transfer coefficients induce a thermal and mass exchange with the internal and external environments. The mc-int and mc-ext curves have similar shapes (Fig.5(a) and (c)), with delicate slope transitions corresponding to the interfaces between mortar and concrete blocks. The moc curve (Fig.5 (a) and (c)), which describes respectively the temperature and humidity distribution in the mortar, is generally similar in trend to the mc-int and mc-ext curves, but with clearly lower values. There are more pronounced deviations between these curves at both boundary of the wall, probably indicating a difference in the hygroscopic behavior of materials near surfaces exposed to the indoor and outdoor environment. The temperature and relative humidity results obtained in the D-SS case are almost similar for the three lines, with a characteristic inflection attributable to the interface effect at the junction between the mortar and the DPC.



(a) (b) (c)
 Fig.4 Temperature (a), water content (b) and Humidity (c) distribution across masonry wall for (D-SS)



(a) (b) (c)
 Fig.5 Temperature (a), water content (b) and Humidity (c) distribution across masonry wall for (N-SS)

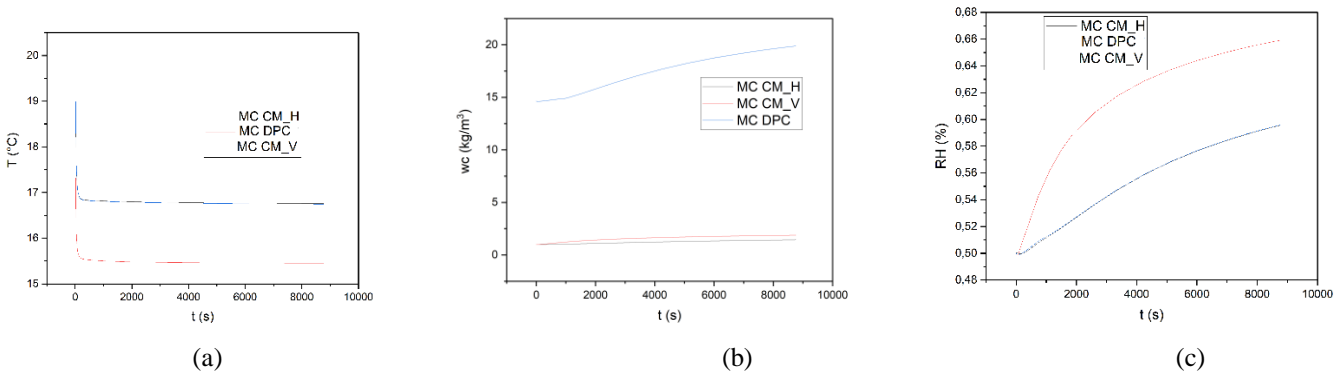


Fig.6 Time-dependent evolution of: Temperature (a), water content (b) and Humidity (c)

Water content, Fig.4(b) and Fig.5 (b), gradually reduces from outside to inside of the wall, showing a natural gradient of moisture where water is transported from wetter to drier conditions. The abrupt falls observed at about 100mm and 300mm indicate material interfaces (concrete blocks and mortar joints) showing capillary discontinuity at these boundaries. The moisture content in DPC blocks (mc-int and mc-ext, up to 55 kg/m³) is significantly greater than in mortar (moc, less than 3 kg/m³), and this suggests that there is a significant difference between the hygroscopic characteristics of the two materials. The shapes of the mc-int and mc-ext curves are the same but shifted, i.e., boundary conditions (interior and exterior) influence moisture distribution in the wall differently. For both D-SS and N-SS cases, slight differences in maximum and minimum values are observed at the wall boundaries. With Dirichlet conditions (Fig.4(b)), the boundary values are strictly imposed, resulting in more defined values at the wall extremities, whereas for the Neumann case (Fig.5(b)), fluxes are imposed, which may lead to slightly different values at the boundaries.

The temperature evolution (Fig.6 (a)) shows initial temperatures of approximately 20°C followed by sharp temperature drops within the first 1000 seconds. MC-DPC stabilizes at approximately 15.5°C while MC-CM-H and MC-CM-V stabilize at approximately 17°C. After this initial stabilization process, temperatures are relatively constant throughout the remainder of the simulation. The water content (Fig.6 (b)) shows that MC-DPC has the highest water content (15-19 kg/m³), rising steadily with time. In contrast, MC-CM-H and MC-CM-V contain considerably lower water contents of approximately 1-2 kg/m³. Horizontal and vertical mortar joints (CM-H and CM-V) experience nearly identical water content behavior throughout the simulation period. The trend of relative humidity development (Fig.6 (c)) presents increasing trends for all the observation points during the time. MC-DPC presents the highest values of relative humidity, with an increase from

about 0.50% to about 0.66%. MC-CM-V presents intermediary values, and MC-CM-H presents the lowest values of relative humidity among the three points. The temperature and relative humidity follow almost the same evolution tendencies for the two points of the vertical and horizontal mortar joints (MC-CM-V and MC-CM-H), while the DPC material has different behavior with lower equilibrium temperature, with much more water content, and with higher relative humidity values. These differences refer to the distinct hygrothermal properties of materials involved in the wall construction and their distinct response to environmental conditions. The DPC appears to have a higher moisture absorption capacity but provides thermal insulation as well, as indicated by its lower temperature overall.

Mortar joints (CM-H and CM-V) show very similar behavior, with much lower values of water content than DPC (between 0.8 and 1.8 kg/m³). Their water content increases very slightly and almost linearly over time, with a much lower slope of increase (around 10 times less pronounced) than that of DPC. Vertical mortar (CM-V) maintains a slightly higher water content than horizontal mortar (CM-H), but this difference remains minimal. However, the water content in the DPC is significantly higher, starting at around 14.5 kg/m³ and reaching almost 20 kg/m³ after 9000 seconds. The curve shows a progressive and continuous increase, without reaching a stabilization plateau during the observation period. The rate of increase is more pronounced, with a relatively constant slope, but which seems to decrease slightly towards the end of the period (suggesting a potential slowdown in absorption).

4. Conclusion

This numerical analysis of heat and mass transport in a cement mortar date palm concrete masonry wall demonstrates that temperature and humidity distribution is strongly dependent on boundary conditions, Neumann conditions producing linear gradients and Dirichlet conditions imposing strict boundary values. The material interfaces are characterized by a significant capillary discontinuity with very much higher water content in concrete blocks (up to 55 kg/m³) than in mortar joints (less than 3 kg/m³). Temperatures in transient analysis come to equilibrium quickly (concrete ~15.5°C, mortar ~17°C), and the water content increases progressively, particularly in concrete. Horizontal and vertical joints of mortar exhibit similar behavior with very small difference. Date palm concrete demonstrates higher moisture absorption capacity and thermal insulation. The focus of this research is on the need for material-specific hygrothermal characteristics in masonry wall design and their influence on building performance in general.

References

- [1] Belloum, R., B. Agoudjil, N. Chennouf, and A. Boudenne, Hygrothermal performance assessment of a bio-based building made with date palm concrete walls. *Building and Environment*, 2022. **223**: p. 109467.
- [2] Ali-Boucetta, T., A. Ayat, W. Laifa, and M. Behim, Treatment of date palm fibres mesh: Influence on the rheological and mechanical properties of fibre-cement composites. *Construction and Building Materials*, 2021. **273**: p. 121056.
- [3] Boumhaout, M., L. Boukhattem, H. Hamdi, B. Benhamou, and F. Ait Nouh, Thermomechanical characterization of a bio-composite building material: Mortar reinforced with date palm fibers mesh. *Construction and Building Materials*, 2017. **135**: p. 241-250.
- [4] Benaimeche, O., A. Carpinteri, M. Mellas, C. Ronchei, D. Scorza, and S. Vantadori, The influence of date palm mesh fibre reinforcement on flexural and fracture behaviour of a cement-based mortar. *Composites Part B: Engineering*, 2018. **152**: p. 292-299.
- [5] Tioua, T., A. Kriker, G. Barluenga, and I. Palomar, Influence of date palm fiber and shrinkage reducing admixture on self-compacting concrete performance at early age in hot-dry environment. *Construction and Building Materials*, 2017. **154**: p. 721-733.
- [6] Abdel-Rahman, H.H., R. Al-Juruf, F. Ahmad, and I. Alam, Physical, mechanical and durability characteristics of date palm frond stalks as reinforcement in structural concrete. *International Journal of Cement Composites and Lightweight Concrete*, 1988. **10**(3): p. 175-181.
- [7] Yahiaoui, W., A. Kenai, B. Menadi, and S. Kenai, Mechanical Performance and Durability of Date Palm Fibers Repair Mortar. *The Open Civil Engineering Journal*, 2022. **16**.

- [8] Belatrache, D., S. Bentouba, N. Zioui, and M. Bourouis, Energy efficiency and thermal comfort of buildings in arid climates employing insulating material produced from date palm waste matter. *Energy*, 2023. **283**: p. 128453.
- [9] Aboudalle, M., F. Meftah, Q.H. Nguyen, B.T.T.H. Le, and M. Sari, Experimental study on the mechanical behavior of the elementary components of masonry walls at high temperature. *Fire Safety Journal*, 2025. **152**: p. 104334.
- [10] Abasi, A., B. Banting, and A. Sadhu, Strength evaluation of early-age full-scale unreinforced masonry walls against out-of-plane loading using experimental and numerical studies. *Engineering Structures*, 2025. **325**: p. 119507.
- [11] Stochino, F., A. Majumder, A. Frattolillo, M. Valdes, and E. Martinelli, Jute fiber reinforcement for masonry walls: Integrating structural strength and thermal insulation in sustainable upgrades. *Journal of Building Engineering*, 2025. **104**: p. 112210.
- [12] Abasi, A., A. Sadhu, K. Dunphy, and B. Banting, Evaluation of tensile properties of early-age concrete-block masonry assemblages. *Construction and Building Materials*, 2023. **369**: p. 130542.
- [13] Ramirez, R., B. Ghiassi, P. Pineda, and P.B. Lourenço, Simulation of moisture transport in fired-clay brick masonry structures accounting for interfacial phenomena. *Building and Environment*, 2023. **228**: p. 109838.
- [14] Zhou, X., D. Derome, and J. Carmeliet, Analysis of moisture risk in internally insulated masonry walls. *Building and Environment*, 2022. **212**: p. 108734.
- [15] Luikov, A.V., Heat and Mass Transfer in Capillary-Porous Bodies, in *Advances in Heat Transfer*, T.F. Irvine and J.P. Hartnett, Editors. 1964, Elsevier. p. 123-184.
- [16] Qin, M., R. Belarbi, A. Ait-Mokhtar, and L.-O. Nilsson, Coupled heat and moisture transfer in multi-layer building materials. *Construction and Building Materials*, 2009. **23**(2): p. 967-975.
- [17] Steeman, M., M. Van Belleghem, M. De Paepe, and A. Janssens, Experimental validation and sensitivity analysis of a coupled BES–HAM model. *Building and Environment*, 2010. **45**(10): p. 2202-2217.
- [18] Liu, Y., Y. Wang, D. Wang, and J. Liu, Effect of moisture transfer on internal surface temperature. *Energy and Buildings*, 2013. **60**: p. 83-91.
- [19] Kuenzel, H., Simultaneous heat and moisture transport in building components. One- and two-dimensional calculation using simple parameters. *Fraunhofer IBP*, 1995.
- [20] Steeman, M., A. Janssens, H.J. Steeman, M. Van Belleghem, and M. De Paepe, On coupling 1D non-isothermal heat and mass transfer in porous materials with a multizone building energy simulation model. *Building and Environment*, 2010: p. 865-877.
- [21] Krejčí, T., J. Kruis, M. Šejnoha, and T. Koudelka, Numerical analysis of coupled heat and moisture transport in masonry. *Computers & Mathematics with Applications*, 2017. **74**(1): p. 229-248.
- [22] Xu, Y., Z. Zeng, and D.a. Sun, Experimental and numerical investigation on the effect of heat and moisture coupling migration of unsaturated lateritic clay for the soil thermal storage system. *Energy and Buildings*, 2022. **276**: p. 112499.
- [23] Lelievre, D., T. Colinart, and P. Glouannec, Hygrothermal behavior of bio-based building materials including hysteresis effects: Experimental and numerical analyses. *Energy and Buildings*, 2014. **84**: p. 617-627.
- [24] Wang, X., X. Jin, Y. Yin, X. Shi, and X. Zhou, A transient heat and moisture transfer model for building materials based on phase change criterion under isothermal and non-isothermal conditions. *Energy*, 2021. **224**: p. 120112.
- [25] Li, Q., J. Rao, and P. Fazio, Development of HAM tool for building envelope analysis. *Building and Environment*, 2009. **44**(5): p. 1065-1073.
- [26] Janssen, H., B. Blocken, and J. Carmeliet, Conservative modelling of the moisture and heat transfer in building components under atmospheric excitation. *International Journal of Heat and Mass Transfer*, 2007. **50**(5): p. 1128-1140.
- [27] Fang, A., Y. Chen, and L. Wu, Modeling and numerical investigation for hygrothermal behavior of porous building envelope subjected to the wind driven rain. *Energy and Buildings*, 2021. **231**: p. 110572.
- [28] Remki, B., K. Abahri, M. Tahlaïti, and R. Belarbi, Hygrothermal transfer in wood drying under the atmospheric pressure gradient. *International Journal of Thermal Sciences*, 2012. **57**: p. 135-141.
- [29] Ayres de Mello, L., L.M. Moura, and N. Mendes, A model for assessment of heat and moisture transfer through hollow porous buildings elements. *Case Studies in Thermal Engineering*, 2019. **14**: p. 100446.

- [30] Ayres de Mello, L., L.M. Moura, and N. Mendes, A model for predicting heat, air and moisture transfer through fibrous materials. *International Journal of Thermal Sciences*, 2019. **145**: p. 106036.
- [31] Kaoutari, T. and H. Louahlia, Experimental and numerical investigations on the thermal and moisture transfer in green dual layer wall for building. *Case Studies in Thermal Engineering*, 2024. **53**: p. 103946.
- [32] Dong, W., Y. Chen, Y. Bao, and A. Fang, A validation of dynamic hygrothermal model with coupled heat and moisture transfer in porous building materials and envelopes. *Journal of Building Engineering*, 2020. **32**: p. 101484.
- [33] Othmen, I., P. Poullain, A. Caucheteux, and N. Leklou, Sensitivity analysis of the Kunzel model: application to the study of the hygrothermal transfer in a tuffeau wall. *WIT transactions on engineering sciences*, 2014. **83**: p. 417-428.
- [34] Maděra, J., V. Kočí, J. Kočí, and R. Černý, Physical and mathematical models of hygrothermal processes in historical building envelopes. Vol. 1906. 2017. 140003.
- [35] Bendekhis, M., N. Fezzioui, M. Benyamine, O.A. Osra, M.A. Alkhafaji, A.M. Dikandé, N. Kaid, Y. Menni, and A.J. Chamkha, Finite element analysis of hygrothermal interactions in date palm concrete, autoclaved aerated concrete, and gypsum walls using the Kunzel model under arid and hot Climate. *International Journal of Low-Carbon Technologies*, 2025. **20**: p. 323-333.
- [36] Brocken, H.J.P., *Moisture transport in brick masonry: the grey area between bricks*. 1998.
- [37] Janssen, H., H. Derluyn, and J. Carmeliet, Moisture transfer through mortar joints: A sharp-front analysis. *Cement and Concrete Research*, 2012. **42**(8): p. 1105-1112.
- [38] Ramirez, R., B. Ghiassi, P. Pineda, and P.B. Lourenço, Hygro-Thermo-Mechanical Analysis of Brick Masonry Walls Subjected to Environmental Actions. *Applied Sciences*, 2023. **13**(7): p. 4514.
- [39] Alioua, T., B. Agoudjil, N. Chennouf, A. Boudenne, and K. Benzarti, Investigation on heat and moisture transfer in bio-based building wall with consideration of the hysteresis effect. *Building and Environment*, 2019. **163**: p. 106333.